Article

Resolving Hierarchical Structures in Carbon Nanotube Networks Using Small and Ultra-Small Angle Neutron Scattering

Mehran Tehrani, Thusitha Nanda Bandara Etampawala, Mark D. Dadmun, and Mohammad Abir Hossain

J. Phys. Chem. C, **Just Accepted Manuscript** • DOI: 10.1021/acs.jpcc.7b06114 • Publication Date (Web): 04 Sep 2017

Resolving Hierarchical Structures in Carbon Nanotube Networks Using Small and Ultra-Small Angle Neutron Scattering

Mehran Tehrani[a,*] Tusitha Nanda Bandara Etampawala[b,c], Mark Dadmun[c,d] and Mohammad Abir Hossain[a]

[a] Advanced Structural and Energy Materials Laboratory, Department of Mechanical Engineering, University of New Mexico, Albuquerque, New Mexico, Unite States

[b] Center for Instrumentation Facility, Faculty of Applied Sciences, University of Sri Jayewardenepura, Nugegoda, Sri Lanka

[c] Chemistry Department, University of Tennessee, Knoxville, Tennessee, United States

[d] Chemical Sciences Division, Oak Ridge National Laboratory, Oak Ridge, Tennessee, United States

[*] Corresponding author. Tel: 505 277-6298. E-mail: mtehrani@unm.edu (Mehran Tehrani)

Abstract

Resolving hierarchical structures in carbon nanotube (CNT) composites is crucial for their performance optimization. We report here that self-consistent analyses of small- and ultra-small-angle neutron scattering (SANS and USANS, respectively) patterns can be used to extract both the size and morphology of the hierarchical structures in carbon nanotube networks. In particular, this study investigates the correlation of structure and electrical conductivity of CNT-PEDOT:PSS (poly(3,4-ethylenedioxythiophene):poly(styrenesulfonate)) composite films where distinguishable dispersion states of nanotubes in the PEDOT:PSS matrix were achieved by varying the CNT concentration, duration of sonication, and addition of ethylene glycol (EG) to the pre-deposition solutions. It was concluded that five hierarchical levels of structure, spanning a few nanometers to tens of microns, exist in all samples. The results suggest a strong variation in the structure of the nanocomposites at larger length scales and, to a lesser extent, at smaller length scales with the variation in processing. Electrical conductivity of samples was largely affected by the morphological changes at larger scales. The EG addition affected the electrical conductivity by both increasing the matrix conductivity and improving CNT dispersion. The presented analysis is also useful for the characterization of structures in pure CNT and low CNT composite samples.

1 Introduction

Polymer nanocomposites based on low dimensional fillers, such as nanotubes, offer a great opportunity to achieve materials with superior mechanical and physical properties. Carbon nanotubes (CNTs), in particular, have found many applications including but not limited to structural composites,[1] conductive plastics and electromagnetic interference shielding coatings,[2] artificial muscles,[3] multifunctional and smart fibers and yarns,[4] and energy storage and conversion devices such as supercapacitors, fuel cells, batteries, and solar cells.[5] Nanotubes are usually used as a filler in a host matrix and their volume fractions are small (i.e., < 5 vol.%).[1, 6] In some of their more recent applications such as organic thermoelectrics[7] and CNT muscles,[3] however, much higher CNT loadings are required to achieve a desired function. In almost all these applications, whether in a polymer composite or in the form of a yarn or film, carbon nanotube networks possess a hierarchical structure that spans nanoscale to microscopic dimensions.[8-11] Our current understanding of single-walled CNT (SWCNT) structures is that they are comprised of different building blocks at different length scales. At the nanoscale these include individual single-walled carbon nanotubes (usually ~1-5 nm), SWCNT bundles (<100 nm, i.e., several side-by-side nanotubes) and pores/polymers confined in between the bundles. Larger structures such as flocs (an aggregate of bundles), different cross-linking blocks, and larger structurally ordered morphologies may exist depending on the system composition and processing.[12] Structure of multi-walled CNT (MWCNT) networks maybe somewhat different.[13] The morphology and connectivity of these hierarchical structures determine properties of CNT systems, and therefore it is crucial to develop methods for their characterization and establish processes for controlling them.[14] In respect to the former, electron microscopy has been widely

used for the characterization of CNT structures.

Cross-sectional scanning and transmission electron microscopy (SEM and TEM, respectively) can provide a reliable representation of the bulk morphology if the material system under investigation has a simple structure, e.g., dispersion of spherical nanoparticles in a medium.[15] For more complex structural systems, automated layer-by-layer removal of the sample followed by microscopy imaging can be used to reconstruct the 3D structure of the sample.[16] This method is suitable for resolving microstructures in a bulk sample. One disadvantage of this approach is the possibility of altering the sample surface and thus the structure due to material removal procedures. Moreover, removing material from the surface at the nanometer scale is both challenging and time-intensive. Alternatively, X-ray computed tomography (XCT) could be used as a non-destructive method to reveal the internal bulk structure of relatively large samples with resolutions that are larger than 50 nm.[17] Recently, energy-filtered electron tomography was used to resolve the 3D nano-morphology of nanotubes in an aligned CNT nanocomposite sample.[18] This method, 3D TEM tomography, was successfully used to extract volume fraction and alignment of CNTs, bundle/network topology, and detailed 3D waviness of aligned CNT samples.[18] Areas as large as 150 by 150 microns and maximum sample thickness of 220 nm were examined;[18] TEM samples must be transparent to electrons and are therefore thinner than a few hundreds of nanometers.

In general, monitoring CNT morphology specifically at the nanoscale (1-100 nm) can be realized using both real space imaging (e.g., electron microscopy) and reciprocal space analysis (e.g., scattering).[19] The former is a very powerful technique to elucidate structures and morphologies on the nano- and micron length scales. Microscopy techniques, however, only provide a 2D slice of CNT network morphology of a specific area/volume and do not contain

sufficient statistical information of the 3D bulk structure of the material. Scattering, on the other hand, gives ensemble structural information averaged over relatively large volumes, of the bulk sample, carrying detailed quantitative information.[9, 11-12] Extracting detailed morphological information from scattering curves requires fitting of the data using a realistic structural model. Microscopy observations can aid with choosing an appropriate model.[20] Microscopy and scattering are therefore complimentary for structural characterization.

Both X-ray and neutron scattering have been used to study the morphology of polymers and carbon nanotubes in solutions as well as low volume fraction CNT composites.[8-9, 21-24] X-ray diffraction is widely used for quantifying the alignment in pure CNT fibers and sheets.[25-28] For CNT-polymer composites, however, neutrons provide excellent contrast between the proton-rich polymer and proton-poor CNT to evaluate the interfaces, structure, and morphology. Small and ultra-small neutron scattering (SANS and USANS, respectively) can be therefore utilized to capture structural information over a range of length scales (~1 nm to 30 μm) that span polymer-nanotube interfaces, individual nanotubes, and aggregates of nanotubes in the samples. SANS also enables characterization of the interface between different phases where the roughness of the interface and existing features are commensurate with the length scales visible to neutrons.[29]

This study investigates the structure and electrical conductivity of CNT-PEDOT:PSS (poly(3,4-ethylenedioxythiophene):poly(styrenesulfonate)) composite films where distinguishable dispersion states of CNTs in the PEDOT:PSS matrix was achieved by varying the CNT concentration (10, 30, and 50 wt.%), duration of sonication (10 minutes, 6 hr and 42 hr) and addition of 5 vol.% ethylene glycol (EG) to the pre-deposition solutions. PEDOT:PSS is a conducting polymer and is used in many energy storage and conversion applications. This water-soluble polymer was used as both the surfactant (used to disperse nanotubes) and the conducting

matrix to increase the electrical conductivity of our CNT composites. CNT-conducting polymer nanocomposites are a relatively new class of nanocomposites, comprised of complex and hierarchical structures that necessitate a more detailed characterization of their dispersion and morphology. Ultra-sonication duration was used here to gradually vary the dispersion of the CNT networks in an aqueous solution of PEDOT:PSS. Changes in the morphology and composition of PEDOT:PSS were also realized through adding Ethylene Glycol (EG) to the pre-deposition CNT-polymer solution.[30] Addition of EG to the pre-deposition solution has been shown to increase carrier density[31] and modify the morphology of PEDOT:PSS chains,[32] thus altering the overall properties of the CNT-PEDOT:PSS nanocomposites.[33-34] The scattering of PEDOT:PSS-CNT is analyzed as a two-phase system, where the PEDOT:PSS matrix is treated as a single phase, due to the large contrast between CNT and PEDOT:PSS, and minimal contrast between PEDOT and PSS. Electrical conductivity for the different samples were measured and correlated to the structural sizes extracted from SANS and USANS analyses. This study, for the first time, reveals the potential of SANS and USANS for the detailed characterization of structure in nanocomposites with high CNT loadings. The presented analysis is also useful for pure CNT samples as well as composites with low CNT contents.

2 Materials and methods

2.1 Materials and Processing

PEDOT:PSS in the form of a 1.3% aqueous solution (PEDOT to PSS by weight ratio of 1:2.5) was purchased from Heraeus, brand name Clevios™ PH 1000. Nano-C PT-100 single-walled carbon nanotube (SWCNT) were purchased from Nano-C, Inc. According to Nano-C, these nanotubes were purified to >85% (10-15 % amorphous carbon), possessed a length of 1-1.1

microns, a diameter of 0.9-1.3 nm, and contained less then 3% iron/iron oxide. Nanotubes were used without further processing. Analytical grade Ethylene Glycol (EG) from Sigma-Aldrich was used for solvent treatments.

PEDOT:PSS is known to disperse CNTs in aqueous solutions. All solutions were prepared by adding the desired amount of nanotubes to 15 ml of Clevios PH1000 solution. 5 vol.% EG was added to some of these solutions. The EG addition changes the morphology of the PEDOT:PSS chains and results in orders of magnitude increase in conductivity of the resulting PEDOT:PSS films. The solution was stirred using a glass rod and sonicated subsequently in a temperature controlled ultrasonication bath for 10 minutes, 6 hours, or 42 hours. Sonication durations were carefully chosen to achieve three distinguishable dispersion states. Samples were then poured into polycarbonate flat containers and left under the fume hood to dry. Samples were post-cured at 80 °C for 4 hours in vacuum to ensure complete solvent removal. Samples containing 10, 30 or 50 wt.% CNTs were fabricated. Produced films were ~5 cm in diameter and ~40 microns thick. Square samples of 1x1 cm were cut for measurements. Surfaces of the pure PEDOT:PSS films were very smooth. For the CNT containing samples, surface roughness increased with CNT loading and decreased with sonication time; the 50 wt.% sample sonicated for 10 mins had the roughest surface due to the many agglomerates existing in the sample whereas the 10 wt.% CNT samples sonicated for 42 hr had a highly smooth surface similar to that of the pure PEDOT:PSS samples.

2.2 Characterization

An FEI Q3D scanning electron microscope (SEM) was used to acquire cross-sectional micrographs of samples. For SEM imaging, samples were immersed in LN2, fractured immediately after, and used without any further processing. The in-plane electrical conductivity

of films was measured using the four-terminal method. To ensure good contact between the sensors and the film, four silver stripes were placed on the specimen where the probes made electrical contact. Data acquisition and instrument control were performed via a LabVIEW interface. A Keithley Current Source Model 6220 and a Nanovoltmeter Model 2182A were used to source current and measure voltages, respectively.

UV-Vis-NIR absorption spectrum of different CNT solutions was measured using a Cary 4000 series UV-Vis-NIR absorption spectrometer. Solutions were diluted to 0.01 mg CNT per 1 ml of water and for each solution background absorption was corrected using solutions containing no CNT but identical amount of PEDOT:PSS.

Raman spectrum of CNT-PEDOT:PSS samples was collected using an Alpha 300R WITec confocal Raman microscope and signal was averaged out over a 5x5 microns area.

2.3 SANS and USANS Experiments

SANS data was collected at the high flux isotope reactor (HFIR) at the Oak Ridge National Laboratory (ORNL) and USANS was collected at the National Institute of Standards and Technology (NIST) center for neutron research. The resulting SANS and USANS curves were analyzed to quantify the structure of the examined nanocomposites. The measurements were collected over a wide Q range ($Q=4\pi/\lambda \sin[\theta/2]$), where λ is the neutron wavelength and θ is the scattering angle. The scattering data were collected over the 0.003 $Å^{-1}$ to 0.60 $Å^{-1}$ Q range.

The Beaucage model[35] was used to elucidate the hierarchical structures in samples. This model assumes the material is comprised of N number of domains where each domain contains two components with the first representing the size of a scattering domain (R_g) and the second

representing an interfacial scaling power (p) of the domain. The unified Beaucage equation correlates scattering intensity, I, to wave vector, Q, as follows:

$$I(Q) = \sum_{i=1}^{N} \left[G_i exp\left(-Q^2 R_{g,i}^2/3\right) + B_i \left[\frac{erf\left(QR_{g,i}/\sqrt{6}\right)^3}{Q} \right]^{P_i} \right] + \mathrm{B}$$

where each level consists of a Guinier and power law scattering behavior. N is the hierarchical level, G_i and B_i are the pre-factors for the two components in a given level, R_g is the radius of gyration of the level, P_i is the power of the interfacial term in the level, and B is the incoherent background. This model can be challenging to use as there are four fitting parameters per level.

3 Results and discussion

The specific sonication times of 10 min, 6 hr, and 42 hr were chosen to achieve three distinguishable CNT dispersion states in the pre-deposition solution. The UV-Vis absorption can be used as a means to quantify dispersion (solubility) of particles in a solution. In particular the absorption at 500 nm can be used to qualitatively measure SWCNT dispersion in different solutions, as absorption in this region corresponds to the metallic transitions of the SWCNTs.[36] As shown in Figure **1**, the 10 min, 6 hr, and 42 hr sonication durations of CNTs in PEDOT:PSS solution resulted in highly distinguishable changes of dispersion evident by the dramatic changes in their absorption peak intensity from ~0.1 to ~0.6 to ~1.1, respectively.

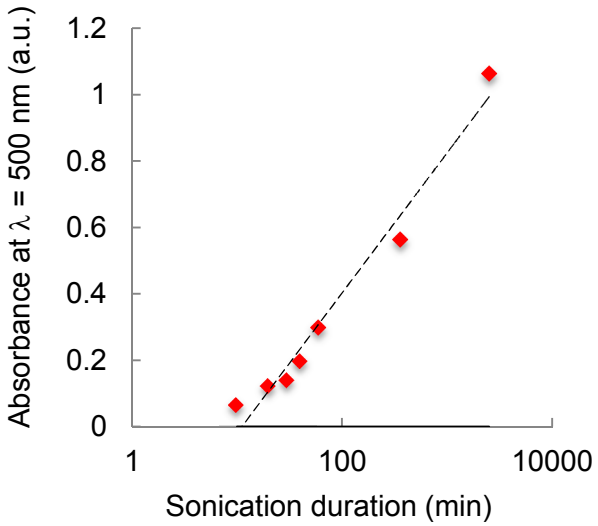

Figure 1. Absorption intensity of CNT solutions at 500 nm wavelength.

Compared with tip sonication, bath sonication has been shown to have little effect on CNT structure. Raman spectroscopy was used to study the structure of CNTs by offering a quantitative measure of the CNT doping, crystallinity, and nanotube diameter. In particular, the D to G band intensity ratios can be used as a measure of CNT damage. The mild bath sonication used in this study did not affect the peak ratios (I_D/I_G ratio of ~0.075) measured after several hours of sonication as shown in Figure **2**. The sample exhibits a very strong radial breathing mode (RBM) at 282 cm^{-1}, hence an average nanotube diameter of 0.9 nm is calculated. It should be noted that there is an extra peak around 1426 cm^{-1}, which is between the D (1342 cm^{-1}) and G (1588 cm^{-1}) peaks, that corresponds to the PEDOT:PSS carbon-carbon bond stretching.

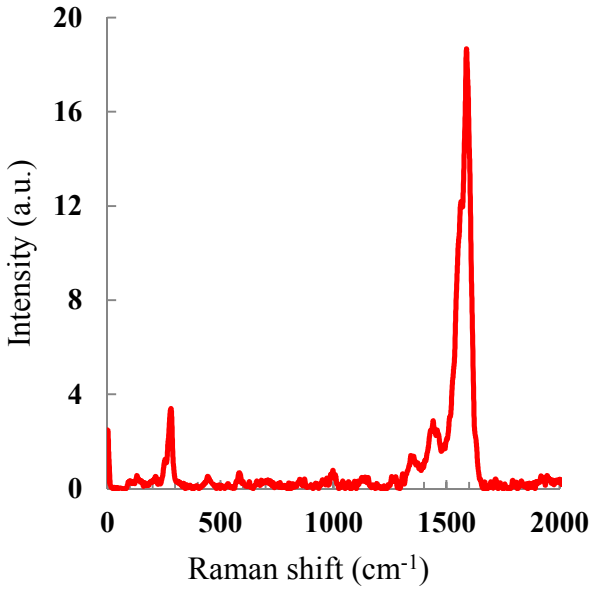

Figure 2. Intensity vs. Raman shift (cm^{-1}) spectrum for the 10 wt.% CNT-PEDOT:PSS sample sonicated for 42 hr.

For all samples, three distinguishable slopes were found in the log-log SANS curves, while only two were present in the log-log USANS data; total of 5 linear regions with distinguishable slopes. This is illustrated for a representative SANS/USANS curve in Figure 3. SANS and USANS curves for all samples is provided in the supplementary document. Each linear region in these plots represents a structural level and the five regions in the scattering curves were analyzed and interpreted as corresponding to different hierarchical structures in the samples. The highest Q region ($\log(Q) > 0.1$) corresponds to the nanostructure of the polymer and is not considered a structural level in this study. The slopes of scattering curves in the low-Q SANS and high-Q USANS regimes (i.e., right and left sides of $\log(Q) = 0.001$, respectively) differ sufficiently to indicate that these two angular regions capture different structural features of the system. The Beaucage model[37-38] was used to monitor the change in CNT aggregate size

as well as size and interfacial structure of the hierarchical assemblies present in the sample.[11, 35, 39] This model has been useful in the analysis of light, X-ray, and neutron scattering of CNT solutions and semi-dilute CNT-polymer samples.[9, 12, 40] Corresponding to the number of hierarchical structures in a given scattering curve, three- and two- level Beaucage models were used for the analysis of SANS and USANS data, respectively.

The linear regions in the log-log plot were fit to a power law using scaling analysis ($I \sim q^{-\alpha}$), where these fits are plotted running through the data in Figure 3. These slopes provide insight into the structures that exist at each length scale, and allow comparisons between the different samples. These slopes were also used in fitting the Beaucage model as a starting parameter for the fitting parameter P_i (scaling exponent). The Beaucage function fit all data sets very well, where the raw data and the corresponding fits are presented in the supporting document (Figure S1).

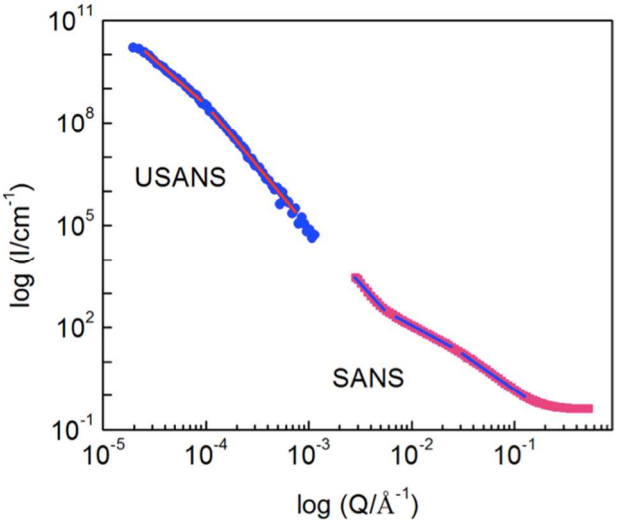

Figure 3. Representative SANS and USANS data exhibiting five distinctive hierarchical structural regions along with the linear fits to each region. Three regions in the SANS data are

referred to as high-, medium-, and low-Q SANS regions. The two regions in the USANS curve are referred to as low- and high-Q regions.

A rod-like structure manifests itself with a slope of -1 in a log(*I*) [scattering intensity] versus log(*Q*) [scattering vector] plot. Such slope has been observed for multi-walled carbon nanotube nanocomposites at very low concentrations (<0.1wt%).[41] SWCNTs, however, almost always form fractal clusters and not rod-like structures across all length scale; this is due to their very high aspect rations, i.e., >1000.[12] The log(*I*) vs. log(*Q*) scattering curves for all the studied samples exhibited slopes smaller than -1.7 in all hierarchical regions, indicating that the SWCNTs in these samples are not individually dispersed, but rather form ropes or bundles that are enmeshed with PEDOT:PSS. This assembly resembles a branched network cluster, where the struts of the network consist of CNT bundles, as shown in Figure 4a. SWCNT (specifically at high concentrations) in a polymer matrix or solvent tend to agglomerate as side-by-side assemblies that are sometimes swollen by a polymer matrix or solvent, Figure 4a and b. [12] These structures may consist of a few to hundreds of SWCNTs. The SWCNT bundles in Figure 4a are on the order of a few tens of nanometers and therefore their structure is captured in the medium-Q SANS region. The distinguishable structural features in the high-Q SANS regions are assigned to tightly packed CNTs, not swollen by any polymer, which will be referred to as nanofibrils here. The bundles (Figure 4b) are swollen by the PEDOT:PSS whereas the nanofibrils (Figure 4c) are likely not. Schaefer proposed a similar hierarchical structure for the SWCNT bundles.[12] These structural features have been observed under TEM by different groups.[42-43] These structural features will be discussed in further details hereafter.

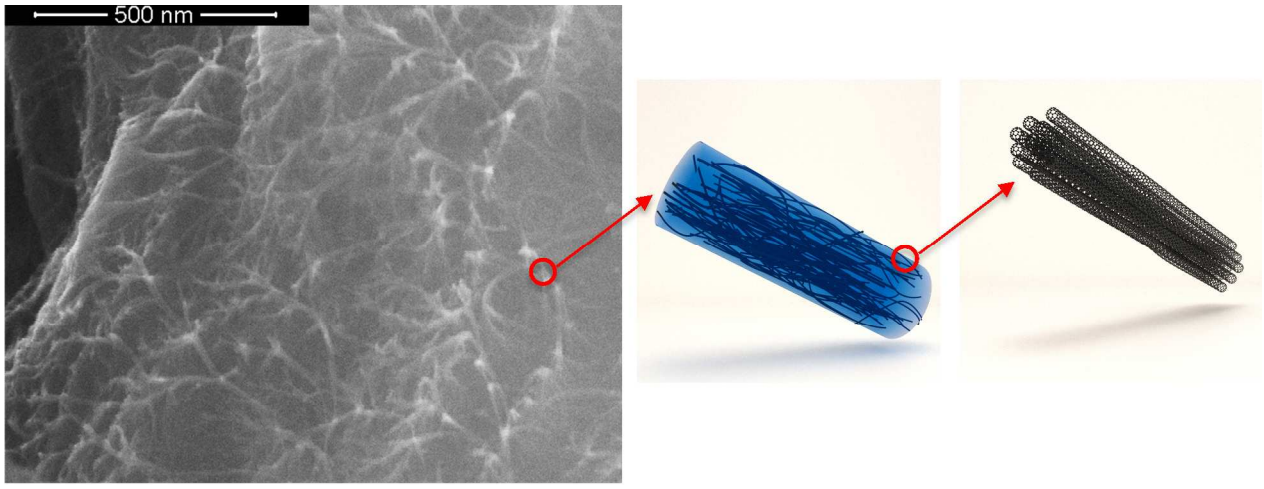

a b c

Figure 4. a) Scanning electron microscopy image of a 10 wt.% CNT sample exhibiting a branched CNT network cluster. CNT bundles are a few tens of nanometers and polymer rich regions (mesh) that fill in between the branched bundles are 50-100 nm in this 2D image. b) Schematic of a CNT bundle consisting of c) CNT nanofibrils.

3.1Analysis of the SANS data

The interfacial structure and dimensionality of an object can be extracted from Porod analysis of scattering data, which is applied to the high- and medium-Q SANS data. The interfacial regions in a Log(I) vs. Log(Q) curve, exhibit a scaling exponent (i.e., slope) of -4 if they have a sharp interface while slopes that differ significantly from -4 indicate increasing interfacial roughness. For mass fractals (CNT networks), the scaling exponent is the fractal dimension and typically is between -2 to -3 for a clustered (collapsed) network and -1.67 for a fully swollen chain.[44-45] The fractal dimension quantifies the structural crowdedness (packing or

inversely the degree of swelling) of a structure. These exponents (Porod exponent, i.e., slope of linear fit to log(I) vs. log(Q) curve regions) for the SANS medium-Q range are tabulated in Table 1, where this length scale corresponds to the cross section of CNT bundles (Figure 4b). These data therefore indicate that the packing of the nanotubes on the tens of nm length scale decreases for all samples with sonication time, and as expected increases with CNT loading. Except for the 10 wt.% sample, the addition of EG to the pre-deposition solution significantly decreases the CNT packing in the final film. This may be due to the effective swelling of CNT bundles by EG-doped PEDOT:PSS. In general, ultrasonication appears to unzip the CNT bundles and swells the resultant aggregates, eventually separating CNTs from the bundles. PEDOT:PSS consists of a hydrophilic chain (PSS) that is attached to hydrophobic PEDOT particles (PEDOT has a much smaller molecular weight compared to PSS). PEDOT can interact with CNTs via π-π stacking and prevent nanotube rejoining after they have been ultrasonically separated. When EG is added to the solution, the effective dielectric constant of the mixture changes; the dielectric constant of water is ~ 80.1 and that of EG is 37.0.[46] Consequently, the amount of PSS that is required to stabilize PEDOT in the solution decreases, which appears to result in a rearrangement of the PEDOT chains morphology from a coil to an extended coil or linear structure [47], observed by a dramatic change in the conductivity of the resulting films. Morphological changes in PEDOT:PSS due to solvent treatment have been recently investigated by the authors.[32] Extended PEDOT chains, as a result of EG addition, are speculated to interact more with CNTs and therefore better stabilize/disperse them.

For a given processing protocol, an increase in CNT concentration leads to the formation of larger aggregates due to the van der Waal forces between CNTs, which in turn increases the packing density (i.e. fractal dimension) of the CNT bundles. Evident by the ~-2.5 mass fractal

dimension, samples containing 50 wt.% CNTs were not swollen by sonication in PEDOT:PSS solution, and in contrary, the 10 wt.% samples that were sonicated for 42 hr were effectively swollen and their bundles expanded. Porod exponents larger than -1.9, underlined in Table 1, can be used a qualitative measure of effective CNT network swelling. Simultaneous use of EG and elongated sonication times can ensure effective CNT dispersion for all CNT loadings.

Table1: The Porod exponents (average mass fractal dimensions) at medium-Q region of SANS profiles. A slope of -2.5 is for a clustered network whereas -1.67 is for a fully swollen chain.[9, 20, 45]

Sonication time	**10wt%**	
	Pure	**EG treated**
10min	-1.835±0.003	-1.871±0.002
6hrs	-1.747±0.003	-1.857±0.003
42hrs	-1.696±0.005	-1.798±0.001
	30wt%	
10min	-2.272±0.003	-1.998±0.004
6hrs	-2.139±0.002	-1.877±0.003
42hrs	-2.068±0.003	-1.812±0.001
	50wt%	
10min	-2.563±0.002	-2.134±0.002
6hrs	-2.538±0.002	-1.893±0.001
42hrs	-2.519±0.001	-1.831±0.003

The radii of gyration (R_g) of the various hierarchical structures as determined from the fits of the Beaucage model to the SANS data are plotted in **Error! Reference source not found.**. The high-Q SANS regime, monitors the local structure of the nanofibrils, and thus this parameter monitors the cross section of a few strongly attached CNTs, i.e., that of the nanofibrils. The R_g in this regime hardly changes with either sonication time or CNT loading, demonstrating a strong van der Wall interaction between side-by-side assembled SWCNTs. Nanofibrils in the samples that were cast from a pure aqueous solution appear to consist of ~25 single CNTs while the ones from the aqueous solution that also contained EG appear to consist of ~20 CNTs, assuming nanofibrils have a circular cross-section where $d = 2\sqrt{2}R_g$, CNT diameter is 1 nm and d is the diameter of the nanofibrils. All R_g values in this regime are within 2% of one another. This confirms the ineffectiveness of bath sonication in altering interfaces between individual nanotubes.

The second hierarchical structural level corresponds to the medium-Q range in SANS data, and represents CNT bundles that are swollen with PEDOT:PSS (except for the ones in the 50 wt.% sample with no EG), where each CNT bundle comprises nanofibrils, as illustrated in Figure 4b. The radius of gyration for these bundles therefore monitors the diameter of the bundles in Figure 4b. Assuming a circular cross-section, bundles in the different samples have a diameter between 21-37 nm. These results therefore show that ultra-sonication debundles the loosely bound CNT nanofibrils, presumably allowing PEDOT:PSS into the gaps between CNT bundles. At low CNT loadings, the changes in the size of these bundles are very clear; however, the effectiveness of the debundling due to sonication is less pronounced with increasing CNT loading. As expected, the extent of debundling increases with increasing sonication time.

The last hierarchical structures that are captured in the SANS data, in the low-Q data, monitor the size of the polymer rich-regions (i.e., the mesh observed in Figure 4a) that separate the CNT bundles. The data presented in **Error! Reference source not found.** show that increased sonication causes an increase in the dispersion of CNTs, which corresponds to a decrease in the mesh size. Similarly, increasing CNT loading results in a decrease in mesh size due to the higher volume fraction of CNTs in the polymer. **Error! Reference source not found.** shows that the change in the mesh size due to ultrasonication is more pronounced at lower CNT loadings. For example, 6 hours of sonication results in a 15% change in the mesh size of the sample with 10 wt.% CNT, whereas there is only a 5% change in the mesh size for the 50 wt.% samples for the same duration of sonication.

The analysis of the SANS data shows that the extent of structural changes that occur at the low- and medium-Q length scales with sonication time are more pronounced for lower CNT loadings. Comparison of the results in **Error! Reference source not found.** shows that for all three hierarchical structures that are captured by the SANS experiment, the presence of EG in the pre-deposition solution facilitates the dispersion of the CNTs and results in better dispersion of the CNT bundles. This is due to swelling of PEDOT:PSS chains in water and thus their better interaction with CNT sidewalls. Similarly, the presence of the EG aids in the penetration of the PEDOT:PSS into the CNT bundles and results in smaller bundle and nanofibrils sizes.

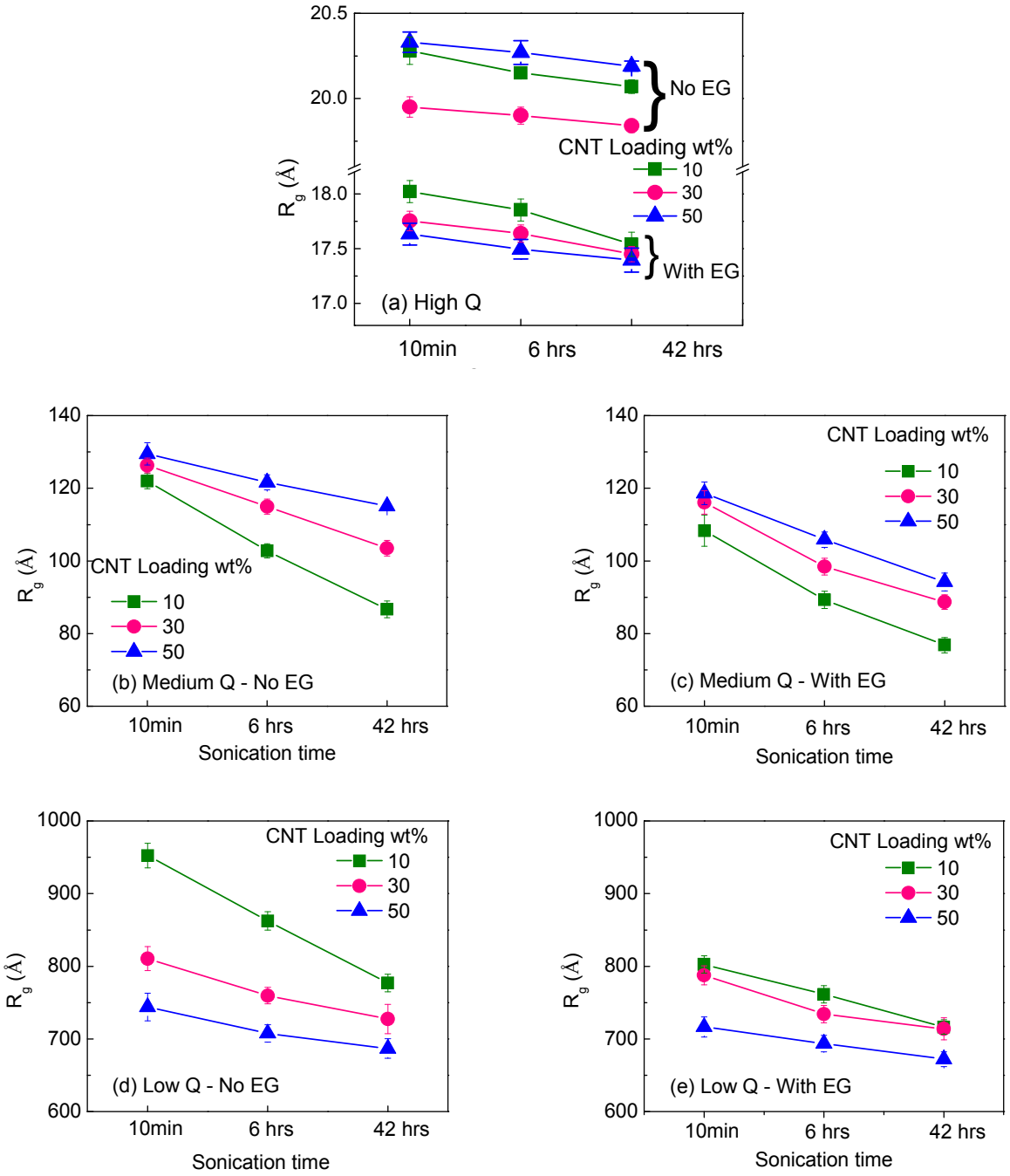

Figure 5. Sonication-time dependence of the dimensions obtained from the three hierarchical levels Beaucage model used for SANS analysis of the samples in presence and absence of EG. With EG means 5 vol.% of EG was added to the solutions prior to the film preparation. No EG means samples were prepared without adding the EG. The dimensions at high-Q, medium-Q and

low-Q are assigned to cross-sections of nanofibrils (a), bundles (b and c) and mesh size (d and e), respectively.

3.2Analysis of USANS Scattering Curves

In addition to the analysis of the SANS data to provide information on the structural features that are on the length scales of a few nm to a few hundred nm, the USANS data provides information on the structural features that exist at even larger length scales from one micron to tens of microns. A representative cross sectional scanning electron microscopy (SEM) image of the nanocomposite with 30 wt.% SWCNT in PEDOT:PSS is shown in Figure 5. This image provides a real space guide to understand the structural features that contribute to the hierarchical structural regions in the USANS scattering curves. This SEM picture shows that the CNT nanocomposites contain two structural features on the length scale of the USANS experiment, both of which take an ellipsoidal shape. This figure also indicates that upon drying, the CNT bundles (flocs) formed in the pre-deposition solutions take a spherical shape (estimated with ellipsoids in the analysis). The size of these flocs is about a few microns as shown in Figure 5. Lastly, these agglomerates surround larger elongated structures with their major axis parallel to the plane of the film (also estimated with ellipsoids in our analysis) that contain the remainder of the PEDOT:PSS that is not in the flocs. These larger structures have an ellipsoidal shape with a major axis length of ~10 microns. These structures take an ellipsoidal shape when dried, which is commensurate with the compressing of the film during drying. All the structural features probed in the SANS and USANS experiments are summarized in

Figure 6.

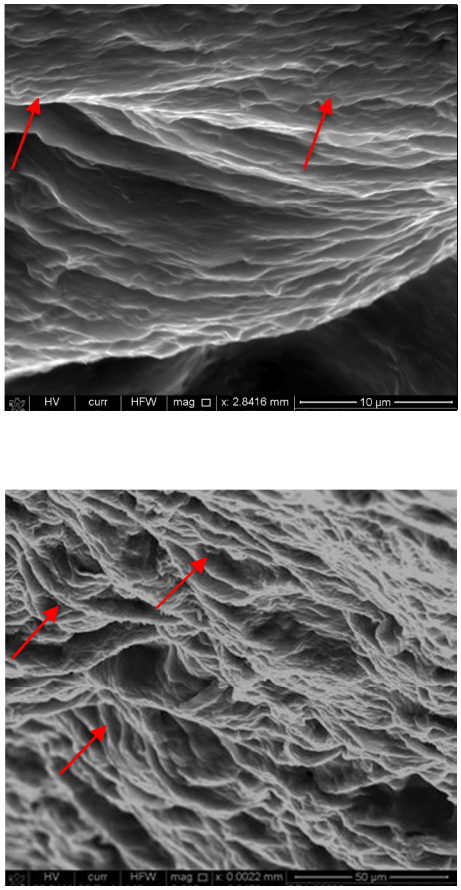

Figure 5. Representative SEM cross-sectional images of 30 wt.% SWCNT loaded PEDOT:PSS sample. The observed structural features were found to be identical for all samples. Corresponding to low-Q USANS region, exhibiting ellipsoidal features and to high-Q USANS, smaller ellipsoidal features. The scale bar in the bottom image is 50 µm and the top is 10 µm.

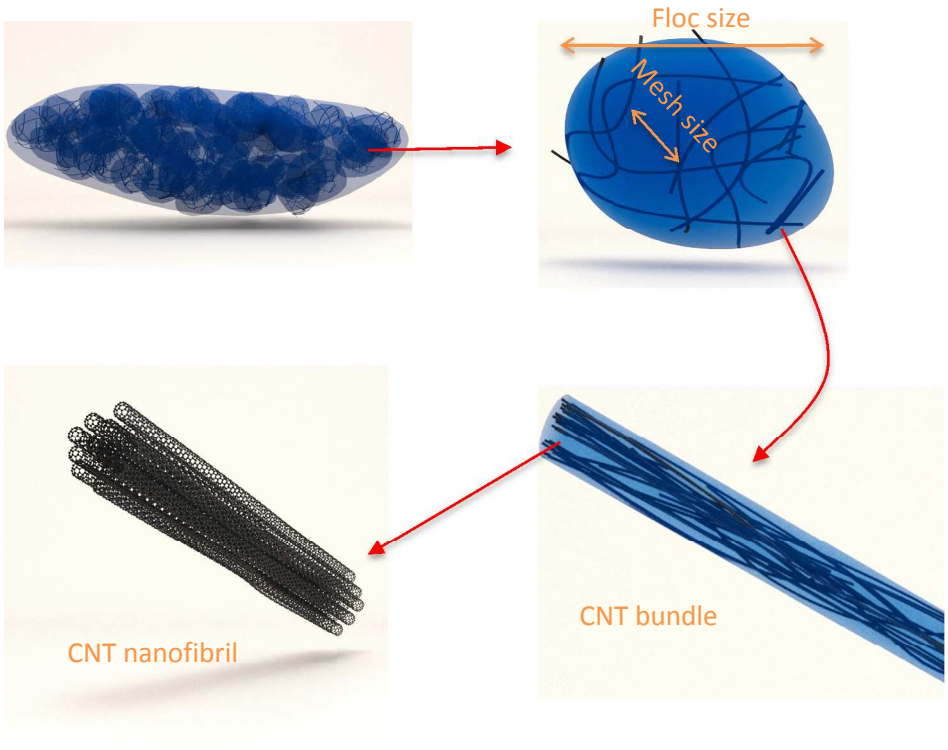

Figure 6. Schematic representation of the hierarchical structural features in the CNT-PESOT:PSS samples probed by SANS and USANS.

As shown in Figure 7, the analysis of the USANS data shows that the size of flocs decrease with both increasing CNT loading and decreasing sonication time. This finding is surprising since longer sonication times usually decrease domain sizes. It may be that this increase is the result of the self-assembly of the bundles driven by the sonication energy. Figure 7 also shows that the floc sizes are in general larger for EG-PEDOT:PSS samples. For the larger ellipsoidal structures (~10 μm in size), both sonication time and CNT loading result in an increase in their size.

Another possible explanation for the changes in structural sizes of meshes and flocs is based on the degree of swelling (how much polymer enters a floc) and CNT debundling. Sonication reduces bundle size, which in turn translates to more bundles in each floc and therefore mesh size is reduced, **Error! Reference source not found.**. For different CNT loadings at any given sonication time, the higher the nanotube loading the more difficult for the polymer to enter the flocs, thus smaller mesh sizes are realized, Figure 7. Similarly, the higher the sonication time the more swollen the floc becomes and therefore floc size increases with sonication time. Finally, for different CNT loadings and at any given sonication duration, floc size is controlled by the amount of polymer that infuses the floc, i.e., the degree of floc swelling. Flocs in higher nanotube loaded samples are more difficult to penetrate by the polymer, their size is therefore reduced by increasing CNT loading.

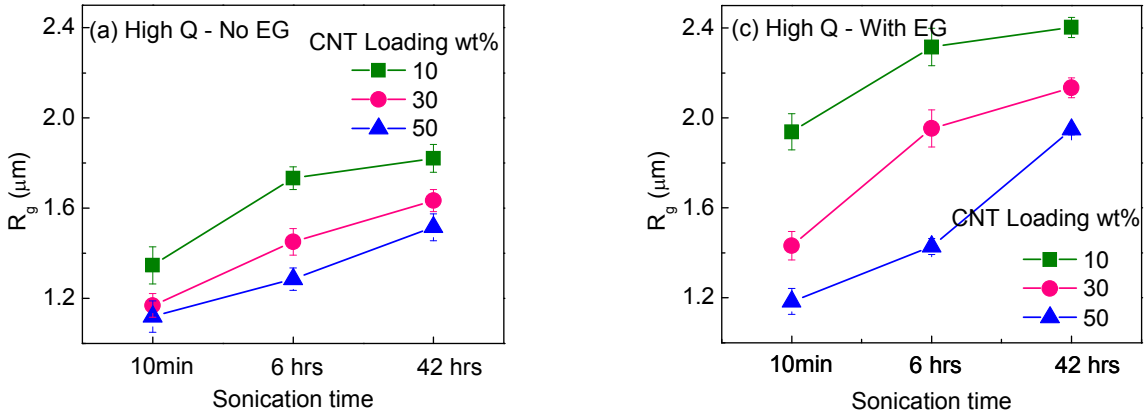

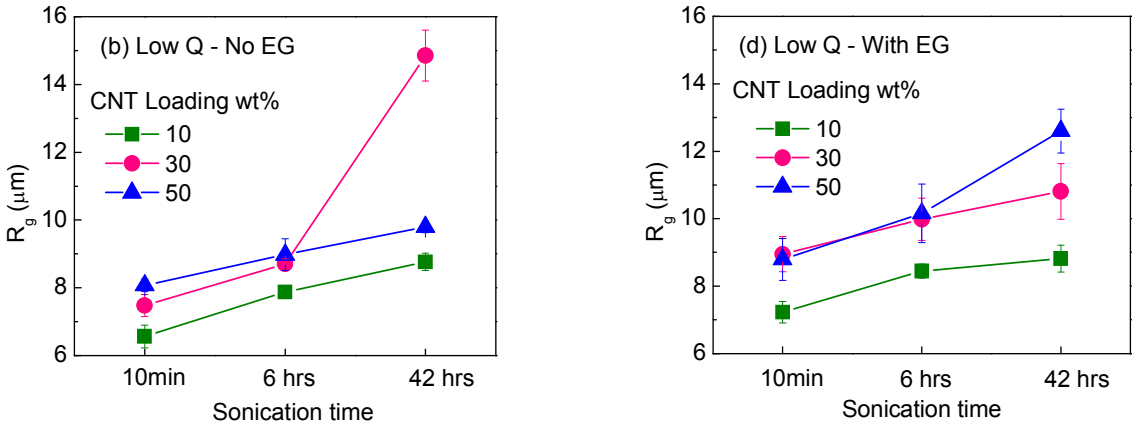

Figure 7. Sonication-time dependence of the dimensions obtained from the two hierarchical levels Beaucage model used for the USANS analysis in the absence of EG: (a) and (b), and in presence of 5 vol.% of EG in the solutions prior to the sample preparation: (c) and (d).

3.3 Structure-Property Relationships

Changes in the electrical conductivity of samples with processing conditions are plotted in Figure 8. The electrical conductivity of the samples fabricated from no-EG solutions increases with CNT concentration and sonication time. Samples treated with EG, however, show a different trend. We propose two different conduction mechanisms in samples fabricated from the no-EG solutions and the EG-treated solutions, respectively. It should be first noted that the conductivity of the matrix in these two sample categories (no-EG and EG samples) are significantly different. The conductivity of PEDOT:PSS film increases from 24.7 to 13,800 S/m upon addition of EG to the pre-deposition solution. This is qualitatively in agreement with recent work that has shown that the increase in conductivity is due to the change in morphology of PEDOT:PSS as well as an increase in its charge carrier density.[31-32] Conduction in no-EG

samples is dominated by the high electrical conductivity of CNTs and their bundles, whereas the conductivity of the EG-treated PEDOT:PSS matrix is on the same order of magnitude as the CNT bundles. As such, charge transport in films occurs through CNT bundles at the floc level and through the PEDOT:PSS rich regions in between the flocs at the film level. Higher sonication time increases CNT debundling, evident by the decrease in nanofibril and bundle size (**Error! Reference source not found.**) with sonication time as well as the increase in swelling degree (Table 1) and the size of the flocs with sonication duration (Figure 7). Conductivity of flocs is much higher compared with the PEDOT:PSS rich regions that connect them and the overall conductivity is therefore limited by the PEDOT:PSS regions connecting the flocs. The low power ultra-sonication negatively affects the electrical conductivity of the no-EG PEDOT:PSS, as shown in Figure **8**. The adverse effect of sonication on PEDOT:PSS conductivity is dominant at lower CNT loadings. This, however, diminishes for the 30 and 50 wt.% CNT samples. This makes sense as the nanotube network dominates charge conduction and therefore for the 30 and 50 wt.% samples, the conductivity increases with sonication time.

Figure **8** results indicate that the EG-treated samples sonicated for 10 mins and 6 hr exhibit an increase in conductivity with sonication time and CNT content. At longer sonication times, this trend is reversed, and can be attributed to the morphological changes in PEDOT:PSS. This is partly due to the fact that sonication in the presence of EG favorably changes the morphology of PEDOT:PSS to achieve higher electrical conductivity. Contrary to the no-EG results, the samples that are deposited from solutions that contain EG exhibit a conductivity that is dominated by that of the matrix (i.e., PEDOT:PSS), where the CNTs only contribute slightly to the increase in the electrical conductivity. This is due to the major differences between the EG and no-EG samples: i) the conductivity of the EG treated PEDOT:PSS matrix is 3 order of

magnitude higher than the no-EG matrix and ii) conductivity of EG-treated PEDOT:PSS increases with sonication time. For the 10 mins and 6 hr sonication time, conduction mechanism is similar to that of no-EG samples explained earlier, due to the fact that the conductivity of the matrix is lower compared with that of the CNT bundles and flocs. For the 42 hr sonicated samples, however, we believe that the conductivity is controlled by the morphology of the PEDOT:PSS rather than the CNT network. PEDOT:PSS morphology is in turn affected by the EG addition, sonication time, and CNT loading and network structure; pure PEDOT:PSS possess the highest conductivity among all samples after 42 hr of sonication. To fully elucidate conduction mechanisms in the EG–treated samples, characterization of the PEDOT:PSS morphology in the presence of nanotubes is required.

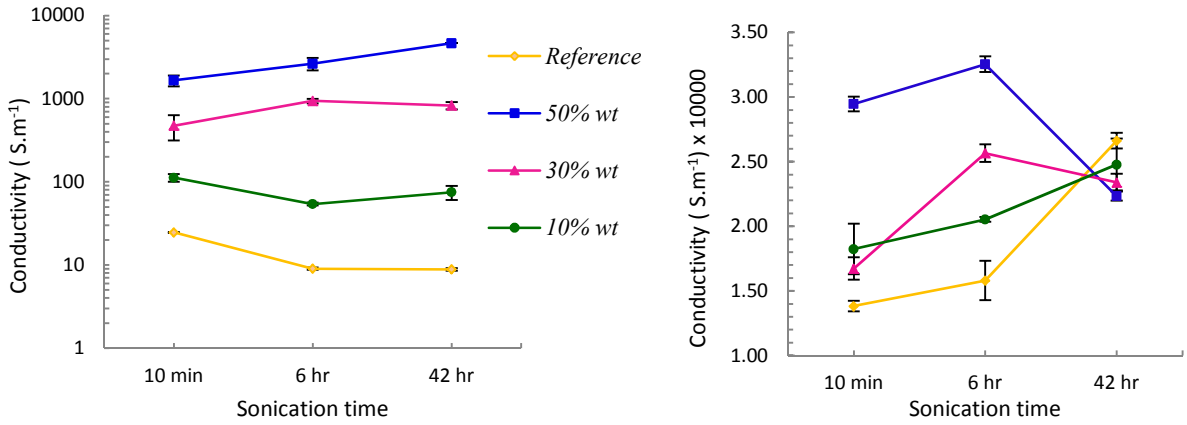

Figure 8. Electrical conductivity of SWCNT - PEDOT:PSS composites at various sonication times. left: no EG treatment and right: EG treatment. Reference sample refers to the neat PEDOT:PSS sample.

4 Conclusions

Structural features in SWCNT-PEDOT:PSS nanocomposites were correlated to their electrical properties. Five structural sizes in the nanometer to micron regimes were identified in all the

samples. Nanoscale structures were a result of nanotube van der Walls interactions, while microscale structures were mostly a result of polymer wrapping around nanotube bundles and drying of the sample in a film form. It is revealed that bath ultrasonication is only slightly effective in disrupting the nanostructure in highly concentrated CNT networks. Unfortunately, harsher dispersion techniques greatly damage CNTs at the price of dispersion and defy the purpose of using highly conductive nanotubes. Conduction in samples not treated with EG was dominated by the conductivity of CNT bundles and flocs. EG treatment increased the conductivity of the matrix by 3 orders of magnitude and therefore conduction was controlled not only by the CNT network structure but also the morphology of the PEDOT:PSS matrix.

Acknowledgments

The authors would like to thank Dr. Huipeng Chen for his help with running the SANS experiments at ORNL and Pouria Khanbolouki for creating the schematics of the CNT structural features. The authors gratefully acknowledge the National Science Foundation (DMR-1409034) for support of this project. A portion of this research was completed at ORNL's High Flux Isotope Reactor, which was sponsored by the Scientific User Facilities Division, Office of Basic Energy Sciences, U.S. Department of Energy. We also acknowledge the support of the National Institute of Standards and Technology, U.S. Department of Commerce, in providing the USANS facilities used in this work, where these facilities are supported in part by the National Science Foundation under Agreement No. DMR-0944772

Supporting Information

SANS and USANS profiles of samples. Analyses of low and high-Q USANS regions.

References

1.Tehrani, M.; Boroujeni, A. Y.; Hartman, T. B.; Haugh, T. P.; Case, S. W.; Al-Haik, M. S., Mechanical Characterization and Impact Damage Assessment of a Woven Carbon Fiber Reinforced Carbon Nanotube-Epoxy Composite. *Compos Sci Technol* **2013**, *75*, 42-48.
2.Verma, P.; Saini, P.; Malik, R. S.; Choudhary, V., Excellent Electromagnetic Interference Shielding and Mechanical Properties of High Loading Carbon-Nanotubes/Polymer Composites Designed Using Melt Recirculation Equipped Twin-Screw Extruder. *Carbon* **2015**, *89*, 308-317.
3.Lima, M. D., et al., Electrically, Chemically, and Photonically Powered Torsional and Tensile Actuation of Hybrid Carbon Nanotube Yarn Muscles. *Science* **2012**, *338*, 928-932.
4.De Volder, M. F. L.; Tawfick, S. H.; Baughman, R. H.; Hart, A. J., Carbon Nanotubes: Present and Future Commercial Applications. *Science* **2013**, *339*, 535-539.
5.Li, L.; Wu, Z.; Yuan, S.; Zhang, X. B., Advances and Challenges for Flexible Energy Storage and Conversion Devices and Systems. *Energ Environ Sci* **2014**, *7*, 2101-2122.
6.Tehrani, M.; Safdari, M.; Al-Haik, M. S., Nanocharacterization of Creep Behavior of Multiwall Carbon Nanotubes/Epoxy Nanocomposite. *Int J Plasticity* **2011**, *27*, 887-901.
7.Moriarty, G. P.; Wheeler, J. N.; Yu, C. H.; Grunlan, J. C., Increasing the Thermoelectric Power Factor of Polymer Composites Using a Semiconducting Stabilizer for Carbon Nanotubes. *Carbon* **2012**, *50*, 885-895.
8.Bauer, B. J.; Hobbie, E. K.; Becker, M. L., Small-Angle Neutron Scattering from Labeled Single-Wall Carbon Nanotubes. *Macromolecules* **2006**, *39*, 2637-2642.
9.Chatterjee, T.; Jackson, A.; Krishnamoorti, R., Hierarchical Structure of Carbon Nanotube Networks. *J Am Chem Soc* **2008**, *130*, 6934-6935.
10.Dumee, L., et al., Characterization of Carbon Nanotube Webs and Yarns with Small Angle X-Ray Scattering: Revealing the Yarn Twist and Inter-Nanotube Interactions and Alignment. *Carbon* **2013**, *63*, 562-566.
11.Mahdavi, M.; Baniassadi, M.; Baghani, M.; Dadmun, M.; Tehrani, M., 3d Reconstruction of Carbon Nanotube Networks from Neutron Scattering Experiments. *Nanotechnology* **2015**, *26*, 385704.
12.Schaefer, D. W.; Justice, R. S., How Nano Are Nanocomposites? *Macromolecules* **2007**, *40*, 8501-8517.
13.Vargas-Lara, F.; Douglas, J. F., Confronting the Complexity of Cnt Materials. *Soft Matter* **2015**, *11*, 4888-4898.
14.Laird, E. D.; Li, C. Y., Structure and Morphology Control in Crystalline Polymer−Carbon Nanotube Nanocomposites. *Macromolecules* **2013**, *46*, 2877−2891.
15.Hanisch, A.; Yang, P. C.; Kulak, A. N.; Fielding, L. A.; Meldrum, F. C.; Armes, S. P., Phosphonic Acid-Functionalized Diblock Copolymer Nano-Objects Via Polymerization-Induced Self-Assembly: Synthesis, Characterization, and Occlusion into Calcite Crystals. *Macromolecules* **2016**, *49*, 192-204.
16.Hasanabadi, A.; Baniassadi, M.; Abrinia, K.; Safdari, M.; Garmestani, H., Efficient Three-Phase Reconstruction of Heterogeneous Material from 2d Cross-Sections Via Phase-Recovery Algorithm. *J Microsc-Oxford* **2016**, *264*, 384-393.
17.Dierolf, M.; Menzel, A.; Thibault, P.; Schneider, P.; Kewish, C. M.; Wepf, R.; Bunk, O.; Pfeiffer, F., Ptychographic X-Ray Computed Tomography at the Nanoscale. *Nature* **2010**, *467*, 436-U82.

18.Natarajan, B.; Lachman, N.; Lam, T.; Jacobs, D.; Long, C.; Zhao, M. H.; Wardle, B. L.; Sharma, R.; Liddle, J. A., The Evolution of Carbon Nanotube Network Structure in Unidirectional Nanocomposites Resolved by Quantitative Electron Tomography. *Acs Nano* **2015**, *9*, 6050-6058.
19.Zhao, J.; Shi, D. L.; Lian, J., Small Angle Light Scattering Study of Improved Dispersion of Carbon Nanofibers in Water by Plasma Treatment. *Carbon* **2009**, *47*, 2329-2336.
20.Natarajan, B., et al., Multiscale Metrologies for Process Optimization of Carbon Nanotube Polymer Composites. *Carbon* **2016**, *108*, 381-393.
21.Dror, Y.; Pyckhout-Hintzen, W.; Cohen, Y., Conformation of Polymers Dispersing Single-Walled Carbon Nanotubes in Water: A Small-Angle Neutron Scattering Study. *Macromolecules* **2005**, *38*, 7828-7836.
22.Golosova, A. A.; Adelsberger, J.; Sepe, A.; Niedermeier, M. A.; Lindner, P.; Funari, S. S.; Jordan, R.; Papadakis, C. M., Dispersions of Polymer-Modified Carbon Nanotubes: A Small-Angle Scattering Investigation. *J Phys Chem C* **2012**, *116*, 15765-15774.
23.Das, N. C.; Yang, K. K.; Liu, Y. Y.; Sokol, P. E.; Wang, Z. G.; Wang, H., Quantitative Characterization of Vertically Aligned Multi-Walled Carbon Nanotube Arrays Using Small Angle X-Ray Scattering. *J Nanosci Nanotechno* **2011**, *11*, 4995-5000.
24.Hernandez, J. J.; Garcia-Gutierrez, M. C.; Nogales, A.; Rueda, D. R.; Ezquerra, T. A., Small-Angle X-Ray Scattering of Single-Wall Carbon Nanotubes Dispersed in Molten Poly(Ethylene Terephthalate). *Compos Sci Technol* **2006**, *66*, 2629-2632.
25.Launois, P.; Marucci, A.; Vigolo, B.; Bernier, P.; Derre, A.; Poulin, P., Structural Characterization of Nanotube Fibers by X-Ray Scattering. *J Nanosci Nanotechno* **2001**, *1*, 125-128.
26.Jiang, C. M.; Saha, A.; Young, C. C.; Hashim, D. P.; Ramirez, C. E.; Ajayan, P. M.; Pasquali, M.; Marti, A. A., Macroscopic Nanotube Fibers Spun from Single-Walled Carbon Nanotube Polyelectrolytes. *Acs Nano* **2014**, *8*, 9107-9112.
27.Ericson, L. M., et al., Macroscopic, Neat, Single-Walled Carbon Nanotube Fibers. *Science* **2004**, *305*, 1447-1450.
28.Zhou, W., et al., Single Wall Carbon Nanotube Fibers Extruded from Super-Acid Suspensions: Preferred Orientation, Electrical, and Thermal Transport. *J Appl Phys* **2004**, *95*, 649-655.
29.Yin, W.; Dadmun, M., A New Model for the Morphology of P3ht/Pcbm Organic Photovoltaics from Small-Angle Neutron Scattering: Rivers and Streams. *Acs Nano* **2011**, *5*, 4756-4768.
30.Kim, G.-H.; Shao, L.; Zhang, K.; Pipe, K. P., Engineered Doping of Organic Semiconductors for Enhanced Thermoelectric Efficiency. *Nature Materials* **2013**.
31.Lin, Y. J.; Ni, W. S.; Lee, J. Y., Effect of Incorporation of Ethylene Glycol into Pedot: Pss on Electron Phonon Coupling and Conductivity. *J Appl Phys* **2015**, *117*, 215501.
32.Etampawala, T.; Tehrani, M.; Nematollahi, A.; He, L.; Dadmun, M., The Impact of Solvent Doping on the Morphology and Performance of Spray-Coated Pedot:Dpss: A Usans and Sans Study. *Organic Electronics* **2017**.
33.Dimitriev, O. P.; Grinko, D. A.; Noskov, Y. V.; Ogurtsov, N. A.; Pud, A. A., Pedot:Pss Films—Effect of Organic Solvent Additives and Annealing on the Film Conductivity. *Synthetic Met* **2009**, *159*, 2237-2239.

34.Kim, Y. H.; Sachse, C.; Machala, M. L.; May, C.; Müller-Meskamp, L.; Leo, K., Highly Conductive Pedot:Pss Electrode with Optimized Solvent and Thermal Post-Treatment for Ito-Free Organic Solar Cells. *Advanced Functional Materials* **2011**, *21*, 1076–1081.
35.Hammouda, B., Analysis of the Beaucage Model. *J Appl Crystallogr* **2010**, *43*, 1474-1478.
36.Bahr, J. L.; Mickelson, E. T.; Bronikowski, M. J.; Smalley, R. E.; Tour, J. M., Dissolution of Small Diameter Single-Wall Carbon Nanotubes in Organic Solvents? *Chemical Communnications* **2001**, 193-194.
37.Beaucage, G., Approximations Leading to a Unified Exponential/Power-Law Approach to Small-Angle Scattering. *J Appl Crystallogr* **1995**, *28*, 717-728.
38.Beaucage, G., Small-Angle Scattering from Polymeric Mass Fractals of Arbitrary Mass-Fractal Dimension. *J Appl Crystallogr* **1996**, *29*, 134-146.
39.Yoonessi, M.; Toghiani, H.; Wheeler, R.; Porcar, L.; Kline, S.; Pittman, C. U., Neutron Scattering, Electron Microscopy and Dynamic Mechanical Studies of Carbon Nanofiber/Phenolic Resin Composites. *Carbon* **2008**, *46*, 577-588.
40.Bauer, B. J.; Hobbie, E. K.; Becker, M. L., Small-Angle Neutron Scattering from Labeled Single-Wall Carbon Nanotubes. *Macromolecules* **2006**, *39*, 2637-2642.
41.Schaefer, D.; Brown, J. M.; Anderson, D. P.; Zhao, J.; Chokalingam, K.; Tomlin, D.; Ilavsky, J., Structure and Dispersion of Carbon Nanotubes. *J Appl Crystallogr* **2003**, *36*, 553-557.
42.Kim, U. J.; Gutiérrez, H. R.; Kim, J. P.; Eklund, P. C., Effect of the Tube Diameter Distribution on the High-Temperature Structural Modification of Bundled Single-Walled Carbon Nanotubes. *J. Phys. Chem. B* **2005**, *109*, 23358–23365.
43.Jeong, S.-H.; Ko, J.-H.; Park, J.-B.; Park, W., A Sonochemical Route to Single-Walled Carbon Nanotubes under Ambient Conditions. *J Am Chem Soc* **2005**, *126*, 15982-15983
44.Teixeira, J., Small-Angle Scattering by Fractal Systems. *J Appl Crystallogr* **1988**, *21*, 781-785.
45.Bale, H. D.; Schmidt, P. W., Small-Angle X-Ray-Scattering Investigation of Submicroscopic Porosity with Fractal Properties. *Phys Rev Lett* **1984**, *53*, 596-599.
46.Akerlof, G., Dielectric Constants of Some Organic Solvent-Water Mixtures at Various Temperatures. *J Am Chem Soc* **1932**, *54*, 4125-4139.
47.Ouyang, J.; Xu, Q. F.; Chu, C. W.; Yang, Y.; Li, G.; Shinar, J., On the Mechanism of Conductivity Enhancement in Poly (3,4-Ethylenedioxythiophene): Poly(Styrene Sulfonate) Film through Solvent Treatment. *Polymer* **2004**, *45*, 8443-8450.

TOC Graphic